Check for updates

Received: 4 May 2023 | Revised: 25 October 2023 | Accepted: 19 November 2023

IET Smart Grid

DOI: 10.1049/stg2.12147

The Institution of Engineering and Technology WILEY

ORIGINAL RESEARCH

Variable DC voltage based reactive power enhancement scheme for MMC-STATCOM

Lujie Yu[1] | Guoyan Wang[1] | Tong Wu[2] | Jiebei Zhu[1] | Campbell D. Booth[3]

[1]School of Electrical and Information Engineering, Tianjin University, Tianjin, China

[2]Langfang Power Supply Company, State Grid Jibei Electric Power Co., Ltd, Langfang, China

[3]Department of Electronic and Electrical Engineering, University of Strathclyde, Glasgow, UK

Correspondence

Jiebei Zhu, No. 92 Weijin Road, Nankai District, Tianjin 300072, China.
Email: jiebei.zhu@tju.edu.cn

Funding information

China State Grid Science and Technology Project, Grant/Award Number: 5100-202155018A-0-00; Science and Technology Project from State Grid Corporation, Grant/Award Number: 52283023000C

Abstract

Constrained by the AC voltage amplitude modulated by a modular multilevel converter-based static synchronous compensator (MMC-STATCOM), its reactive power output may be subject to oscillations under grid contingencies, posing a threat to the grid stable operation. To solve this problem, this paper proposes a variable DC voltage (VDCV)-based reactive power enhancement scheme for MMC-STATCOM. In this scheme, a novel variable DC voltage control is designed, which can increase the DC voltage in a transient state for relaxing the constraint of the AC voltage amplitude modulated by MMC-STATCOM and improving its reactive power output capability (RPC). At the same time, to make full use of the improved RPC of MMC-STATCOM, a VDCV scheme also proposes an optimisation algorithm of its reactive current-AC voltage droop coefficient using the established reactive power model of the MMC-STATCOM. Based on small signal modelling and analysis, the key parameters of the proposed VDCV scheme are optimised. The performance and reactive power enhancement of the VDCV scheme is evaluated through the hardware-in-the-loop experiment under grid disturbances.

KEYWORDS

overvoltage, power system stability, reactive power control, voltage-source convertors

1 | INTRODUCTION

The modular multilevel converter-based static synchronous compensator (MMC-STATCOM) possesses the advantages of fast reactive power regulation speed, wide operation range and low harmonic content [1–4], being proven to be one of the important technologies to guarantee the grid voltage dynamic stability. Especially in the case of grid voltage sags, MMC-STATCOM can provide a certain level of short-term overload capability, output additional reactive power and improve the support effect for the grid voltage in transient states [5, 6]. According to STATCOM design standards and engineering application examples [7, 8], the overload operation time for a STATCOM is allowed in maximum 2s at 1.5 times of its rated current. However, the stability constraints of MMC-STATCOM (e.g., modulation index, submodule capacitor and voltage ripple) may restrict its additional reactive power output. Among them, the modulation index constraint limits the MMC-STATCOM reactive power output to the greatest extent [9–12]. As the MMC-STATCOM enters the overmodulation region, the voltage at the point of common coupling (PCC) can be subject to the high total harmonic distortion (THD) for its distorted modulated AC voltage waveform [13, 14], which may not fulfil the grid-connection codes and other requirements [15–17] (e.g., IEEE Standard 519 recommends that the THD of the PCC voltage should not be more than 3%).

To ensure grid voltage stability, it is necessary to improve the reactive power output capability (RPC) of MMC-STATCOM. The existing research studies focus on increasing the modulation index to expand the amplitude of the modulated AC voltage [18–22]. Directly increasing the modulation index may lead to the overmodulation of the MMC converter station. Moreover, when a modulation index limiter is added to avoid overmodulation [18], the control system may be saturated at its limit, causing the reactive power oscillations of MMC-STATCOM. The modulation strategy of MMC based

This is an open access article under the terms of the Creative Commons Attribution License, which permits use, distribution and reproduction in any medium, provided the original work is properly cited.

© 2023 The Authors. *IET Smart Grid* published by John Wiley & Sons Ltd on behalf of The Institution of Engineering and Technology.

on third-order harmonic voltage injection can effectively expand the modulation index range to increase the amplitude of the modulated AC voltage [19, 20], but its improvement effect can be sensitively affected by the circulating current suppression control [21], and also, the calculation of the third-order harmonic voltage amplitude additionally takes up controller computation resources [22]. In fact, the amplitude of the modulated AC voltage is not only subject to the modulation index but also influenced by its DC voltage [14]. According to the insulation requirements of the MMC-STATCOM DC system, DC voltage can vary within a small range (such as ±10%) around its rated value [10]. Therefore, increasing the DC voltage within an allowable range to increase the modulated AC voltage amplitude can also be an effective manner to improve the RPC of MMC-STATCOM. In this regard, rare relevant work is reported.

The reactive current-AC voltage droop coefficient of MMC-STATCOM is determined by the ratio of the allowable variation range of PCC voltage to the maximum reactive current output [23, 24]. The limited RPC of MMC-STATCOM constrains its maximum reactive current output, resulting in a large droop coefficient and consequently an underutilised regulation on grid voltage. Therefore, with an improved RPC of MMC-STATCOM, its droop coefficient can be further optimised to enhance its regulation effect on the grid voltage. However, the existing literature on improving the RPC of MMC-STATCOM rarely involves the droop coefficient optimisation.

Therefore, this paper proposes a variable DC voltage (VDCV)-based reactive power enhancement scheme for MMC-STATCOM. The main features of the proposed VDCV scheme are summarised as follows:

(1) VDCV scheme designs a novel variable DC voltage control, which can extend the operating range of the modulated AC voltage and improve the RPC of MMC-STATCOM by temporarily raising the DC voltage. Different from third-order harmonic voltage injection schemes in Refs. [19, 20], the VDCV scheme does not require complex calculations, and it also avoid the adverse control impact for improving RPC.
(2) VDCV scheme designs a droop coefficient optimisation algorithm based on an established MMC-STATCOM reactive power model, effectively lowering the droop coefficient and improving its grid voltage regulation effect.

The rest of the paper is as follows: Section 2 introduces the topology and traditional control of MMC-STATCOM. Section 3 establishes the reactive power model of MMC-STATCOM and analyses the limiting factors and potential improvement manners of the MMC-STATCOM RPC. Section 4 proposes the specific VDCV design, including variable DC voltage control and droop coefficient optimizsation. Section 5 optimises the key parameters of the VDCV scheme based on small signal analysis. Section 6 verifies the effectiveness of the VDCV scheme via hardware-in-the-loop experiments. Section 7 summarises the full text.

2 | MMC-STATCOM TOPOLOGY AND TRADITIONAL CONTROL

This section introduces the topology and traditional control of MMC-STATCOM, which provides a theoretical basis to analyse the RPC of MMC-STATCOM and design the novel control.

2.1 | MMC-STATCOM topology

The topology of a three-phase MMC-STATCOM is shown in Figure 1. Each phase of MMC contains the upper and lower arms, and each arm includes an arm inductor (L_0) and N cascaded half-bridge sub-modules (SMs). Each sub-module consists of a DC side capacitor (C) and four semiconductor switching devices (D_1, D_2, S_1, and S_2). The coupling point of the upper and lower arms is connected to PCC via a three-phase transformer (L_t). In Figure 1, u_{pcc} and i are the voltage and current at the PCC, respectively; u_v is the MMC modulated AC voltage; and U_{dc} is the DC voltage. MMC-STATCOM maintains DC voltage stability and realises the modulated voltage output by adjusting the switching state of submodules.

2.2 | MMC-STATCOM traditional control

The MMC-STATCOM traditional control is presented in Figure 2. The outer controller employs constant DC voltage control and reactive current-AC voltage droop control to ensure the stable operation of DC voltage and the PCC voltage, respectively. The inner current controller generates modulation signals for MMC according to the current reference values generated by the outer controller, and adopts a modulation index limiter to avoid MMC from overmodulation. The control system of MMC-STATCOM also includes capacitor voltage balancing control (VBC) and circulating current suppression control (CCSC), which are reported in Ref. [25].

3 | MMC-STATCOM REACTIVE POWER MODEL AND RPC ANALYSIS

This section establishes the MMC-STATCOM reactive power model, analyses its reactive power output constraints and discusses the feasible improvement methods of its RPC.

3.1 | MMC-STATCOM reactive power model and constraints

The equivalent AC circuit of MMC is shown in the grey box of Figure 1. The reactive power flow Q between the MMC and the AC system can be written as:

25152947, 2024, 4, Downloaded from https://ietresearch.onlinelibrary.wiley.com/doi/10.1049/stg2.12147 by NHS Education for Scotland NES, Edinburgh Central Office, Wiley Online Library on [26/08/2024]. See the Terms and Conditions (https://onlinelibrary.wiley.com/terms-and-conditions) on Wiley Online Library for rules of use; OA articles are governed by the applicable Creative Commons License

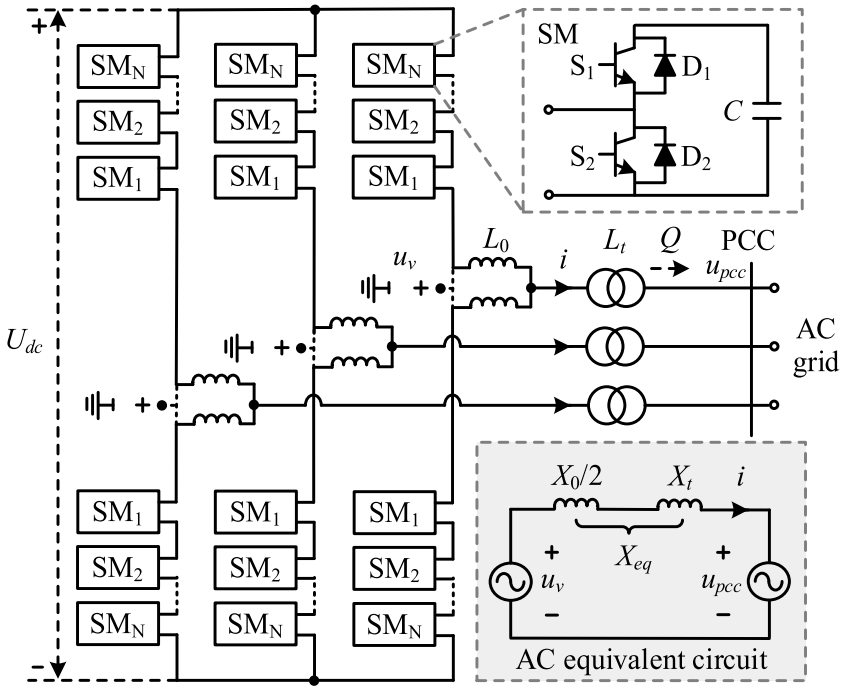

FIGURE 1 MMC-STATCOM topology.

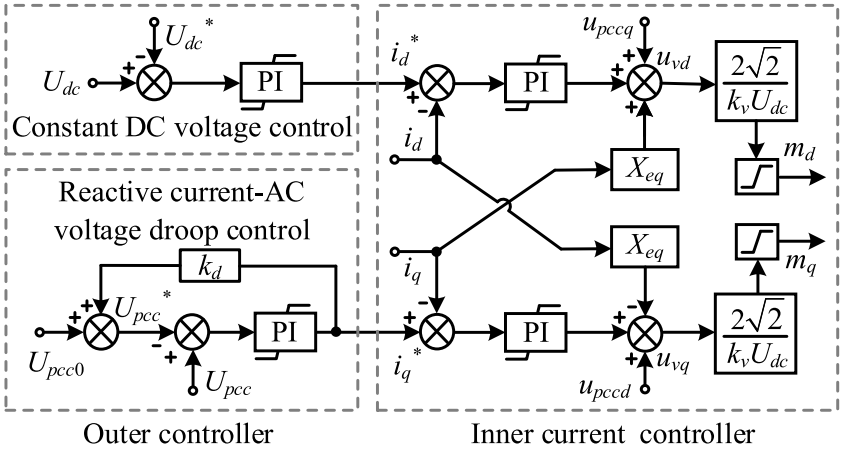

FIGURE 2 MMC-STATCOM traditional control.

$$Q = \frac{U_{pcc}\left(U_v \cos\delta - U_{pcc}\right)}{X_t + X_0/2} \approx \frac{U_{pcc}\left(U_v - U_{pcc}\right)}{X_{eq}} \tag{1}$$

where U_{pcc} and U_v are the RMS value of u_{pcc} and u_v, respectively; X_t and X_0 are the reactances of the transformer and the arm inductor, respectively; X_{eq} is the equivalent reactance between u_{pcc} and u_v; and δ is the phase angle difference between u_{pcc} and u_v ($\delta \approx 0$ as MMC-STATCOM has no active power interaction). To simplify the analysis, all variables in this paper adopt per unit values.

The droop control of MMC-STATCOM characterises the relationship between the PCC voltage reference value U_{pcc}^* and the reactive current reference value i_q^* [23]:

$$U_{pcc}^* = U_{pcc0} + k_d i_q^* \tag{2}$$

where U_{pcc0} is the rated value of U_{pcc}, and k_d is the droop coefficient. In a practical system, the PCC voltage is allowed to fluctuate in a certain range, and the reactive power compensation device can participate in the regulation of the PCC voltage by using a simple reactive current-AC voltage droop control. Meanwhile, some grid connection regulations specify the range of the droop coefficient value for the reactive current-AC voltage droop control [17]. In order to ensure the studied system is consistent with an actual system, this paper adopts reactive current-AC voltage droop control to regulate the PCC voltage. The droop coefficient can be determined by the following equation:

$$k_d = \frac{\Delta U_{\max}}{I_{v\,\max}} \tag{3}$$

25152947, 2024, 4, Downloaded from https://ietresearch.onlinelibrary.wiley.com/doi/10.1049/stg2.12147 by NHS Education for Scotland NES, Edinburgh Central Office, Wiley Online Library on [26/08/2024]. See the Terms and Conditions (https://onlinelibrary.wiley.com/terms-and-conditions) on Wiley Online Library for rules of use; OA articles are governed by the applicable Creative Commons License

where $\Delta U_{\max}$ is the maximum variable range of the PCC voltage, which is generally 0.02–0.07 pu depending on specific grid codes [17]; and $I_{v\max}$ is the maximum reactive current.

The reactive current i_q is given as follows:

$$i_q = -\frac{U_v - U_{pcc}}{X_{eq}} \tag{4}$$

Via proportional-integral (PI) control, the actual values of the aforementioned variables are equal to their reference values in a steady state, thus $U_{pcc} = U_{pcc}^*$ and $i_q = i_q^*$. The relationship between U_{pcc} and U_v can be obtained by combining (2) and (4):

$$U_{pcc} = \frac{X_{eq}U_{pcc0} - k_d U_v}{X_{eq} - k_d} \tag{5}$$

Furthermore, by combining (1) and (5), Q can be written asfollows:

$$Q = \frac{-k_d U_v^2 + (X_{eq} + k_d)U_{pcc0}U_v - X_{eq}U_{pcc0}^2}{(X_{eq} - k_d)^2} \tag{6}$$

According to (6), Q is mainly restricted by U_v when the system parameters X_{eq}, U_{pcc0} and k_d are given, and Q increases with the increase of U_v. The modulated AC voltage limit $U_{v\max}$ is determined by the modulation index limit $m_{\max}$ and DC voltage limit $U_{dc\max}$:

$$U_{v\max} = k_v \frac{m_{\max}U_{dc\max}}{2\sqrt{2}} \tag{7}$$

where k_v is a constant given by U_{dc0}/U_{v0}, where U_{dc0} and U_{v0} are the rated values of DC voltage and the modulated AC voltage, respectively.

Substituting (7) into (6), the maximum reactive power output of MMC-STATCOM under the modulated AC voltage constraint $Q_{v\max}$ can be obtained as follows:

$$Q_{v\max} = \frac{1}{8(X_{eq} - k_d)^2}\left[-k_d(k_v m_{\max}U_{dc\max})^2 + 2\sqrt{2}\,U_{pcc0}(X_{eq} + k_d)k_v m_{\max}U_{dc\max} - 8X_{eq}U_{pcc0}^2\right] \tag{8}$$

Substituting (7) into (5), the maximum reactive power output of MMC-STATCOM under the overload current constraint $Q_{i\max}$ can be obtained as follows:

$$Q_{i\max} = \frac{2\sqrt{2}X_{eq}U_{pcc0} - k_d k_v m_{\max}U_{dc\max}}{2\sqrt{2}(X_{eq} - k_d)} I_{\max} \tag{9}$$

where $I_{\max}$ is the MMC overload current limit.

Considering the two comprehensive RPC constraints of the modulated AC voltage and the overload current limit above, the maximum reactive power output of MMC-STATCOM $Q_{\max}$ is eventually constrained by the smaller value in (8) and (9) as follows:

$$Q_{\max} = \min\{Q_{v\max}, Q_{i\max}\} \tag{10}$$

3.2 | RPC analysis of MMC-STATCOM

Based on the established reactive power model of MMC-STATCOM, this sub-section analyses the RPC of MMC-STATCOM and its possible improvement methods.

The selected parameters k_d, k_v, X_{eq}, U_{pcc0}, and $I_{\max}$ (1.5 times the rated current is adopted in this paper) in (8) and (9) are presented in Table A1. Under the traditional control, $U_{dc\max}$ is normally fixed at 1pu and $m_{\max}$ fixed at 1. Figure 3 shows the three-dimensional relationships of $Q_{v\max}$ or $Q_{i\max}$, $m_{\max}$ and $U_{dc\max}$. It can be observed that $Q_{v\max}$ is far lower than $Q_{i\max}$, indicating that the modulated AC voltage constraint is the main impact factor limiting the RPC of MMC-STATCOM and resulting in the underutilisation of MMC-STATCOM overload capability.

In order to break through the modulated AC voltage constraint and improve the RPC of MMC-STATCOM, it can be seen from Figure 3 and (8) that $Q_{v\max}$ can be significantly improved by increasing $m_{\max}$ or $U_{dc\max}$. The traditional third-order harmonic voltage injection strategy of increasing $m_{\max}$ has complex calculations and is subject to the influence of the circulating current suppression control [19–22], so the VDCV scheme which improves the RPC by increasing the DC voltage is introduced in the following section.

4 | VDCV SCHEME FOR ENHANCING REACTIVE POWER OF MMC-STATCOM

This section proposes a VDCV scheme which includes variable DC voltage control and droop coefficient optimisation. Variable DC voltage control improves the RPC of MMC-

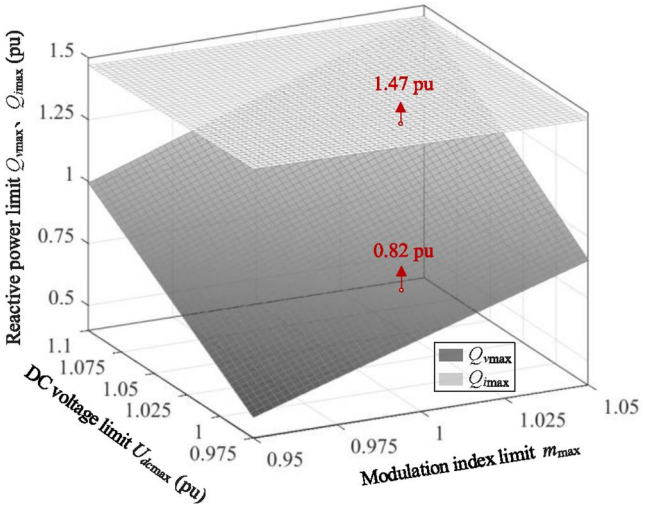

FIGURE 3 Relationships between $Q_{v\max}$, $Q_{i\max}$ and $m_{\max}$, $U_{dc\max}$.

25152947, 2024, 4, Downloaded from https://ietresearch.onlinelibrary.wiley.com/doi/10.1049/stg2.12147 by NHS Education for Scotland NES, Edinburgh Central Office, Wiley Online Library on [26/08/2024]. See the Terms and Conditions (https://onlinelibrary.wiley.com/terms-and-conditions) on Wiley Online Library for rules of use; OA articles are governed by the applicable Creative Commons License

STATCOM by flexibly adjusting the DC voltage, while droop coefficient optimisation reduces the droop coefficient in (3) for a better grid voltage support effect.

4.1 | Variable DC voltage control

To expand the adjustable range of the modulated AC voltage and improve the RPC of MMC-STATCOM, variable DC voltage control adds a modulation index control to adjust the DC voltage reference value U_{dc}^* when modulation index m exceeds its limit $m_{\max}$, which can be expressed as follows:

$$\begin{cases} U_{dc}^* = U_{dc0} + \Delta U_{dc} \\ \Delta U_{dc} = \left(k_p + \dfrac{k_i}{s}\right)(m - m_{\max}), 0 \le \Delta U_{dc} \le \Delta U_{dc\max} \end{cases} \tag{11}$$

where ΔU_{dc} is the correction value of U_{dc}^*; k_p and k_i are the proportional coefficient and integral coefficient of the modulation index control, respectively; and ΔU_{dcmax} is the upper limit of ΔU_{dc}, which is set as 0.1pu in this paper. The lower limit of ΔU_{dc} is set at 0 to prevent the modulation index control being active when unnecessary. The control loop of variable DC voltage control is shown in the red line in Figure 4, and CPS-SPWM generates switching signals to control the switching of sub-modules according to the modulated AC voltage reference signal (the number of MMC-STATCOM sub-modules in this paper is moderate, so CPS-SPWM can be adopted without causing significant loss increase).

4.2 | RPC improvement effect analysis of variable DC voltage control

To evaluate the RPC improvement effect of variable DC voltage control, this section sets up an MMC-STATCOM connected system, as illustrated in Figure 5, and establishes its mathematical model to quantify the RPC of MMC-STATCOM under the proposed control.

The power exchange between the MMC-STATCOM and its connected system is as follows:

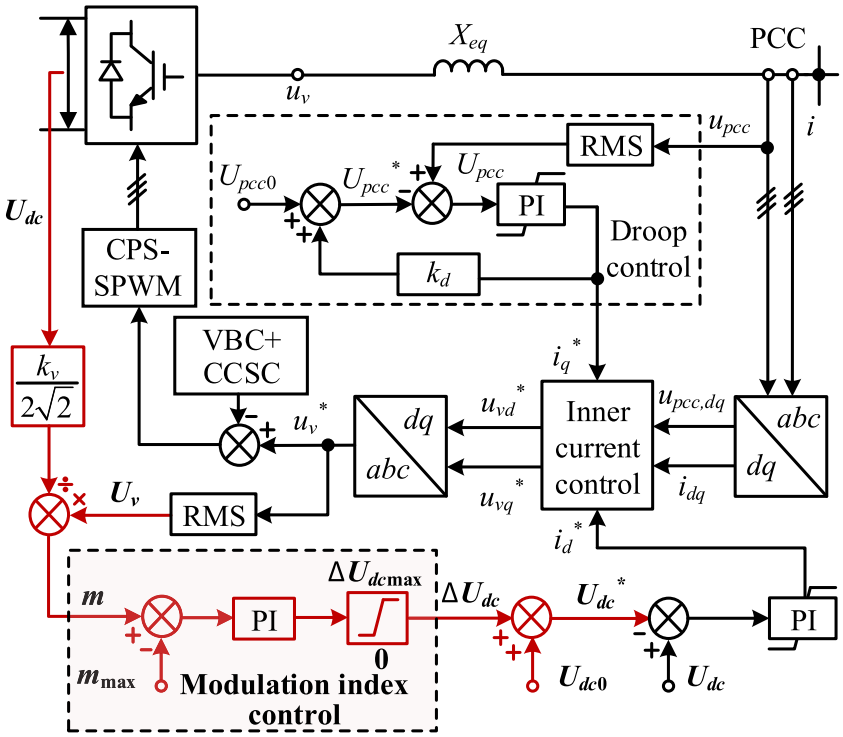

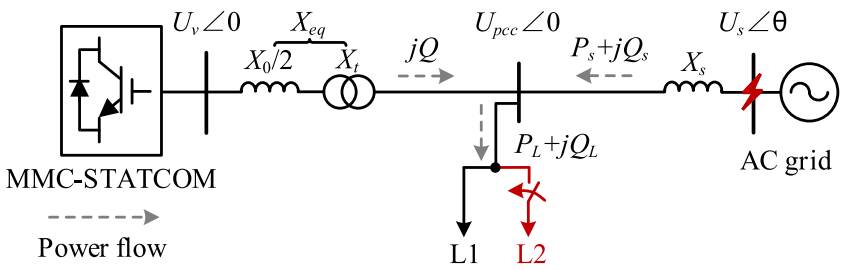

FIGURE 4 Variable DC voltage control.

FIGURE 5 Diagram of the MMC-STATCOM connected system.

25152947, 2024, 4, Downloaded from https://ietresearch.onlinelibrary.wiley.com/doi/10.1049/stg2.12147 by NHS Education for Scotland NES, Edinburgh Central Office, Wiley Online Library on [26/08/2024]. See the Terms and Conditions (https://onlinelibrary.wiley.com/terms-and-conditions) on Wiley Online Library for rules of use; OA articles are governed by the applicable Creative Commons License

$$\begin{cases} P_L = P_s = \dfrac{U_s U_{pcc} \sin\theta}{X_s} \\ Q_L = Q_s + Q = \dfrac{U_{pcc}\left(U_s \cos\theta - U_{pcc}\right)}{X_s} + \dfrac{U_{pcc}\left(U_v - U_{pcc}\right)}{X_{eq}} \end{cases} \tag{12}$$

where U_s is the AC gird voltage; θ is the phase angle difference between U_s and U_{pcc}; X_s is the equivalent reactance of the AC system; $P_L + jQ_L$ is the active and reactive load power; and $P_s + jQ_s$ is the active and reactive power from the AC system.

By combining (5) and (12), the modulated AC voltage U_v can be obtained under specific U_s and $P_L + jQ_L$. Then substituting U_v into (6), the reactive power Q can be obtained accordingly. It is worth stressing that U_v should not exceed its limit $U_{v\max}$ during the substitution to get the correct reactive power output of MMC-STATCOM.

Figure 6 shows the three-dimensional relationship of Q, U_s and Q_L. When U_s is decreased or Q_L is increased within region I, the reactive power output from the MMC-STATCOM Q will be increased with the proposed control, the same as the performances with traditional control. When U_s further decreases or Q_L further increases to Region II, under the traditional control, the reactive power output from the MMC-STATCOM Q reaches its limit and cannot increase as wanted. However, under the proposed variable DC voltage control, Q can further increase since it effectively breaks through the constraint of the modulated AC voltage by increasing the MMC-STATCOM DC voltage.

4.3 | Droop coefficient optimization of MMC-STATCOM

After improving the RPC of MMC-STATCOM by the proposed variable DC voltage control, the optimisation of the droop coefficient k_d in (3) makes it possible to further enhance the voltage regulation effect of MMC-STATCOM. Curve ① in Figure 7 shows the reactive current regulation of MMC-STATCOM under traditional control. The reactive current is regulated following line AB during the change of U_{pcc} and is limited at the maximum reactive current $I_{v\max}$ as in line BC. With the analysis in Section 3, it can be found that $I_{v\max}$ is smaller than the rated reactive current, resulting in a large droop coefficient k_d and weak voltage regulation effect. On the other hand, under variable DC voltage control, the maximum reactive current can be increased to $I_{v\max}'$ as in line ② according to Section 3, so k_d can be correspondingly reduced to fully utilise the improved RPC and enhance the grid voltage regulation effect. Therefore, in this section, the droop coefficient k_d is optimised to identify the slope of line ②.

According to (4), (5), (7), the maximum reactive current $I_{v\max}'$ can be derived as follows:

$$I_{v\max}' = \frac{k_v m_{\max} U_{dc\max}\left(2k_d - X_{eq}\right)}{2\sqrt{2}X_{eq}\left(X_{eq} - k_d\right)} - \frac{U_{pcc0}}{\left(X_{eq} - k_d\right)} \tag{13}$$

It can be observed from (3) and (13) that k_d and $I_{v\max}'$ are mutually effected. Therefore, an iterative method is adopted in this paper to finalise droop coefficient k_d. The optimisation flow chart is presented in Figure 8, and the specific optimisation steps are as follows:

Step 1 Obtain the parameters related to the calculation of droop coefficient k_d, including $\Delta U_{\max}$ in (3), k_v, $m_{\max}$, $U_{dc\max}$, X_{eq} and U_{pcc0} in (13).

Step 2 Solve the optimised droop coefficient through iteration. Firstly, given an initial droop coefficient k_{d0}, obtain $I_{v\max}'$ through (13). Then, substitute $I_{v\max}'$ into (3) to obtain the optimised droop coefficient k_d. Finally, determine whether the

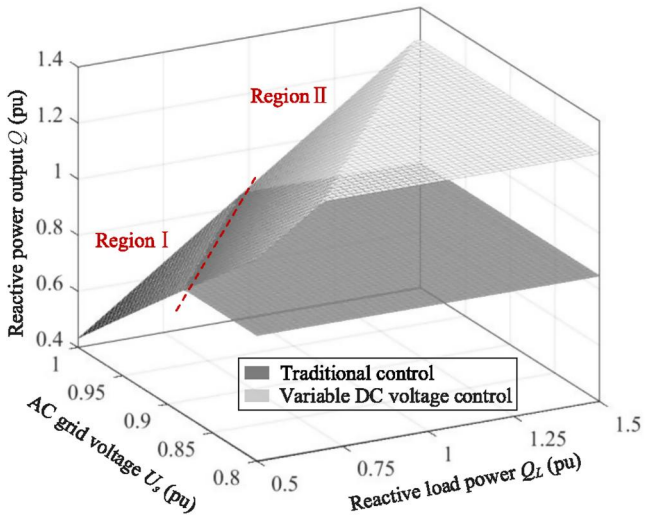

FIGURE 6 Relationship between Q and Q_L, U_s.

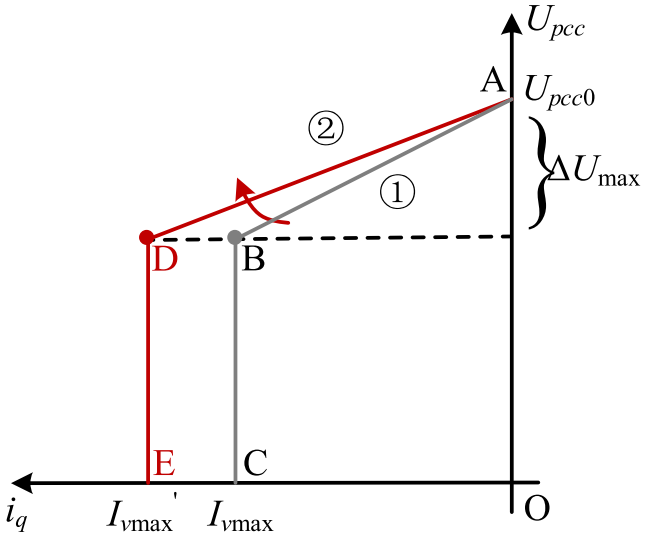

FIGURE 7 Comparison of the MMC-STATCOM droop coefficient before and after optimisation.

25152947, 2024, 4, Downloaded from https://ietresearch.onlinelibrary.wiley.com/doi/10.1049/stg2.12147 by NHS Education for Scotland NES, Edinburgh Central Office, Wiley Online Library on [26/08/2024]. See the Terms and Conditions (https://onlinelibrary.wiley.com/terms-and-conditions) on Wiley Online Library for rules of use; OA articles are governed by the applicable Creative Commons License

absolute value of the difference between k_{d0} and k_d meets the accuracy requirements.

Figure 9 shows the three-dimensional relationship of k_d, $\Delta U_{\max}$ and $U_{dc\max}$. It can be seen from Figure 9 that the droop coefficient k_d under variable DC voltage control (that is, when $U_{dc\max} > 1$) is lower than that under traditional control (i.e., when $U_{dc\max} = 1$). In addition, as seen in Figure 9, with the increase of $U_{dc\max}$, the droop coefficient correspondingly decreases as the RPC of MMC-STATCOM is improved, thereby reducing the drop of the grid voltage.

5 | SMALL SIGNAL ANALYSIS AND PARAMETERS OPTIMIZATION OF VDCV SCHEME

To optimise the key control parameters of the VDCV scheme, a small signal model (SSM) of the MMC-STATCOM connected system as shown in Figure 5 is established in this section. The 47.5 MVar-rated MMC-STATCOM is connected to the AC grid (SCR = 4) through a 32 kV/230 kV step-up transformer. The fixed static load L1 is $S_{L1} = P_{L1} + jQ_{L1} = 28.5\,\text{MW} + j47.5\text{MVar}$. The switchable load L2 is $S_{L2} = jQ_{L2} = j16.63\text{MVar}$ and is switched out in the initial state. The state space equations and specific parameters of the system can be seen in Tables A1 and A2 and Appendix B.

Linearising the state space equations using the linear analysis tool in the Matlab/Simulink platform [26]. The SSM obtained by the linearisation can be expressed as follows:

$$\frac{d}{dt}\Delta \boldsymbol{X} = \boldsymbol{A}\Delta \boldsymbol{X} + \boldsymbol{B}\Delta \boldsymbol{U} \tag{14}$$

where Δ is the small disturbance variation; $\boldsymbol{X}$ is the state column vector; $\boldsymbol{A}$ is the state matrix; $\boldsymbol{B}$ is the input matrix; and $\boldsymbol{U}$ is the input column vector.

To verify the accuracy of SSM, its dynamic responses are compared with those of its time-domain electromagnetic transient (EMT) model in Figure 10. At $t = 0.1$s, the reactive load step increases by 16.63MVar, and the responses of SSM are accurately aligned with those from the EMT model, which verifies the correctness of SSM.

The eigenvalues of the MMC-STATCOM connected system are listed in Table C1 in which modes $\lambda_{7,8}$ and $\lambda_{11,12}$ with low damping ratio are identified as the dominant modes to be focused.

The parameters k_p and k_i of the modulation index control are optimised in this paper. When k_p increases from 0 to 10, as shown in Figure 11a, $\lambda_{7,8}$ move away from the imaginary axis, which indicates the increase of the damping ratio and the improvement of the system stability. $\lambda_{11,12}$ firstly move away from the imaginary axis and then approach it with the increase of k_p and enter the right half plane after k_p exceeds 2.5, which indicates the unstable of the system. Considering the comprehensive influence of k_p on $\lambda_{7,8}$ and $\lambda_{11,12}$, the optimal $k_p = 0.5$ is selected, for the damping ratio of $\lambda_{11,12}$ is the largest and $\lambda_{7,8}$ is far away from the imaginary axis. With the optimal k_p, the oscillation and overshoot of the modulation index response can be significantly suppressed under the step increase of reactive load power, as shown in Figure 11b.

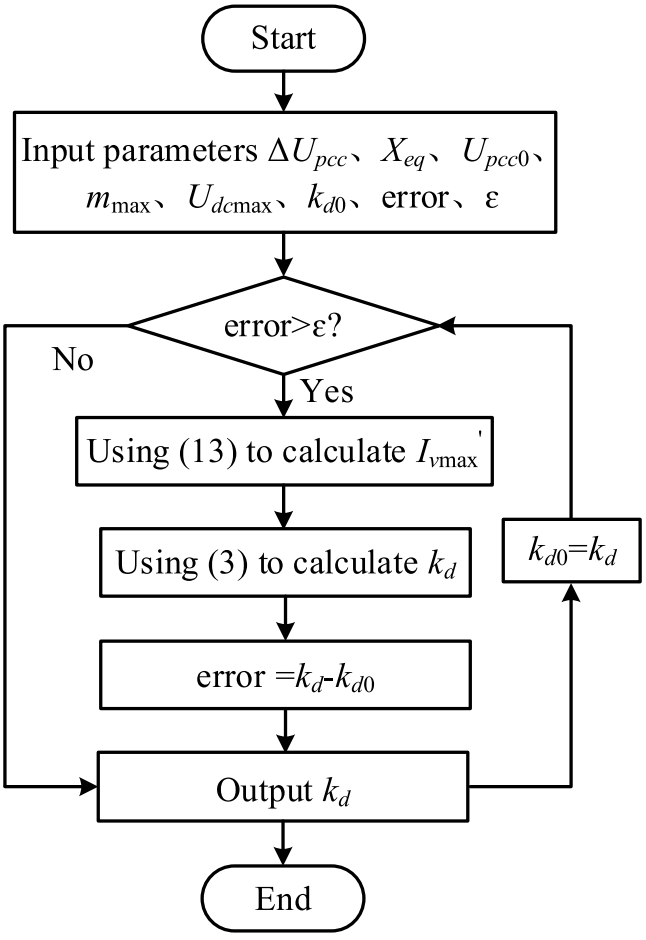

FIGURE 8 The flow chart of droop coefficient optimisation.

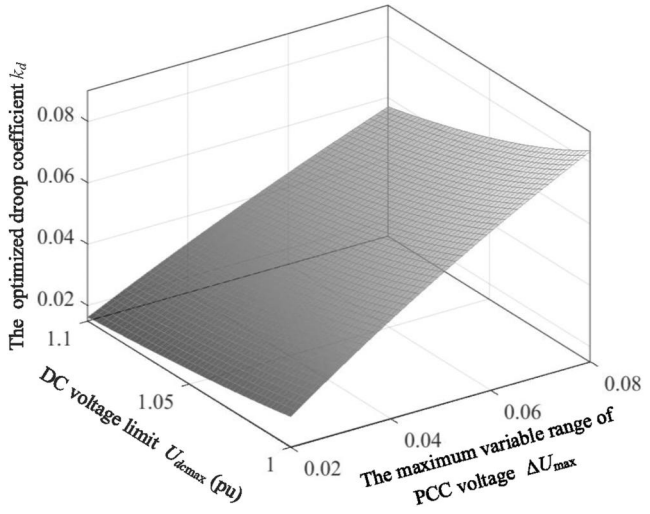

FIGURE 9 Relationship between k_d and $\Delta U_{\max}$, $U_{dc\max}$.

25152947, 2024, 4, Downloaded from https://ietresearch.onlinelibrary.wiley.com/doi/10.1049/stg2.12147 by NHS Education for Scotland NES, Edinburgh Central Office, Wiley Online Library on [26/08/2024]. See the Terms and Conditions (https://onlinelibrary.wiley.com/terms-and-conditions) on Wiley Online Library for rules of use; OA articles are governed by the applicable Creative Commons License

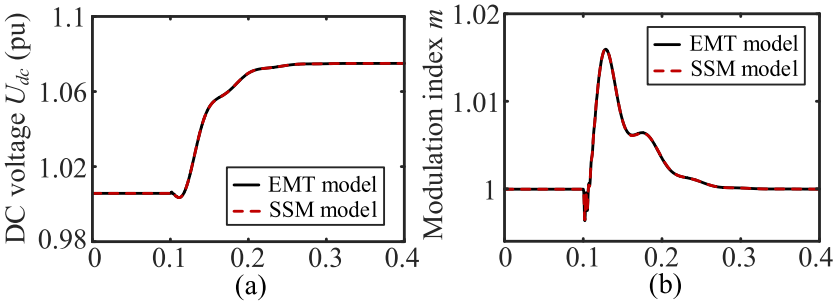

FIGURE 10 Step response comparison between the EMT model and SSM model: (a) DC voltage U_{dc} and (b) Modulation index m.

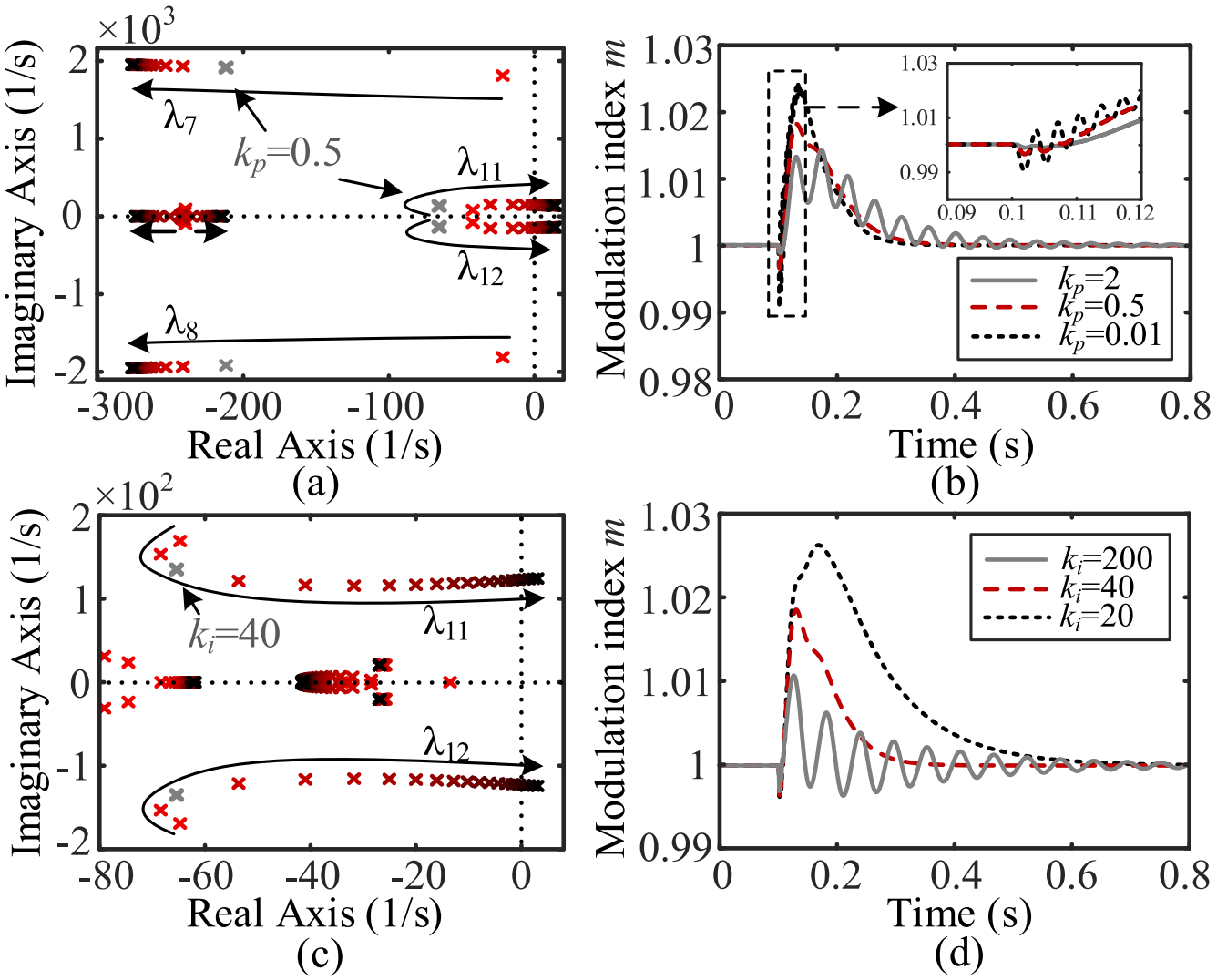

FIGURE 11 Dominant eigenvalue loci and modulation index response under different k_p and k_i: (a) k_p varies from 0 to 10, (b) Modulation index response, (c) k_i varies from 0 to 400, (d) Modulation index response.

When k_i increases from 0 to 400, as shown in Figure 11c, $\lambda_{11,12}$ firstly move away from the imaginary axis and then approach it, resulting in a continuous decrease in a damping ratio. $\lambda_{11,12}$ cross the imaginary axis when k_i increases to 320, leading to system instability. The optimal $k_i = 40$ is selected as its damping ratio is the largest. With the optimal k_i, the modulation index oscillation can be effectively suppressed, and the response speed can be ensured under the step increase of reactive load power, as shown in Figure 11d.

6 | HARDWARE-IN-THE-LOOP EXPERIMENTAL RESULTS

To verify the effectiveness of the VDCV scheme, a hardware-in-the-loop experimental platform of the MMC-STATCOM connected system as shown in Figure 12 is set up in this section. The experimental platform consists of a dSPACE SCALAXIO processing system for MMC-STATCOM control and an RT-LAB OP5600 simulator for the real-time simulation of

25152947, 2024, 4, Downloaded from https://ietresearch.onlinelibrary.wiley.com/doi/10.1049/stg2.12147 by NHS Education for Scotland NES, Edinburgh Central Office, Wiley Online Library on [26/08/2024]. See the Terms and Conditions (https://onlinelibrary.wiley.com/terms-and-conditions) on Wiley Online Library for rules of use; OA articles are governed by the applicable Creative Commons License

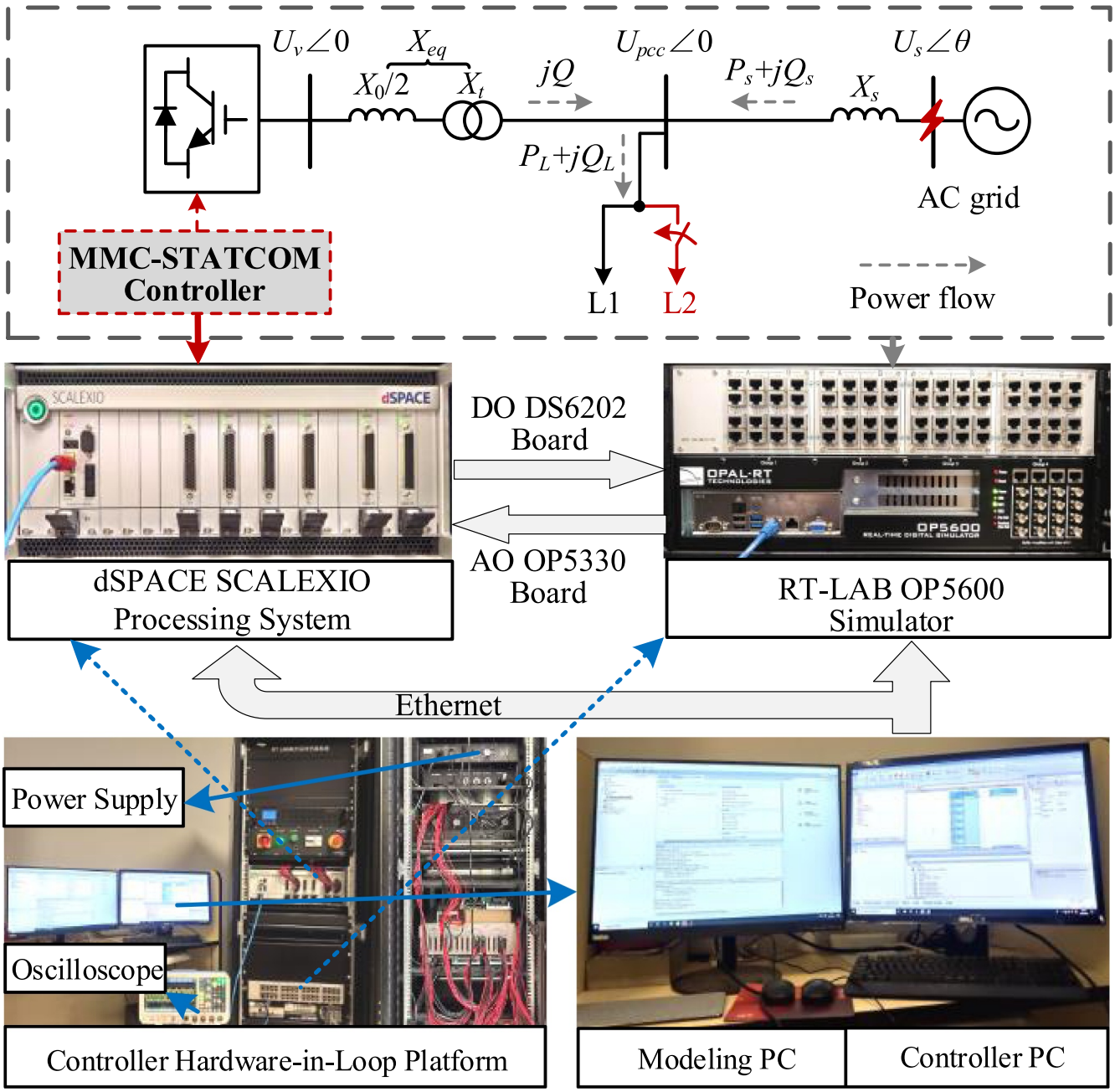

FIGURE 12 MMC-STATCOM connected system and controller-hardware-in-the-loop experimental platform.

the MMC-STATCOM connected system. The performances of the following three schemes on the grid voltage support is compared and analysed under the scenarios of the reactive load step and AC grid three-phase ground fault. The three schemes consist of

1) Traditional control scheme 1 (TC1): The traditional control introduced in Section 2, which has the modulation index limiter and k_d is set as 0.045;
2) Traditional control scheme 2 (TC2): The traditional control without the modulation index limiter and k_d is set as 0.045;
3) Proposed VDCV scheme, and k_d is set as 0.032 according to the optimisation algorithm in Section 4.

6.1 | Scenario 1: reactive load step

Reactive load L2 (as seen in Figure 12) is switched in at $t = 0.1$s, and the system response is illustrated in Figure 13. The increase of the reactive load causes the PCC voltage to decrease, as shown in Figure 13a. It can be observed from Figure 13b that TC1 limits the modulation index at its limit through the modulation index limiter, thus triggering the oscillation of the DC voltage, as shown in Figure 13c. The modulation index limiter of TC1 also causes the low-frequency oscillation and even divergence of the reactive power and the instability of the PCC voltage, as shown in Figures 13a,f. The modulation index exceeds its limit in TC2, and MMC-

25152947, 2024, 4, Downloaded from https://ietresearch.onlinelibrary.wiley.com/doi/10.1049/stg2.12147 by NHS Education for Scotland NES, Edinburgh Central Office, Wiley Online Library on [26/08/2024]. See the Terms and Conditions (https://onlinelibrary.wiley.com/terms-and-conditions) on Wiley Online Library for rules of use; OA articles are governed by the applicable Creative Commons License

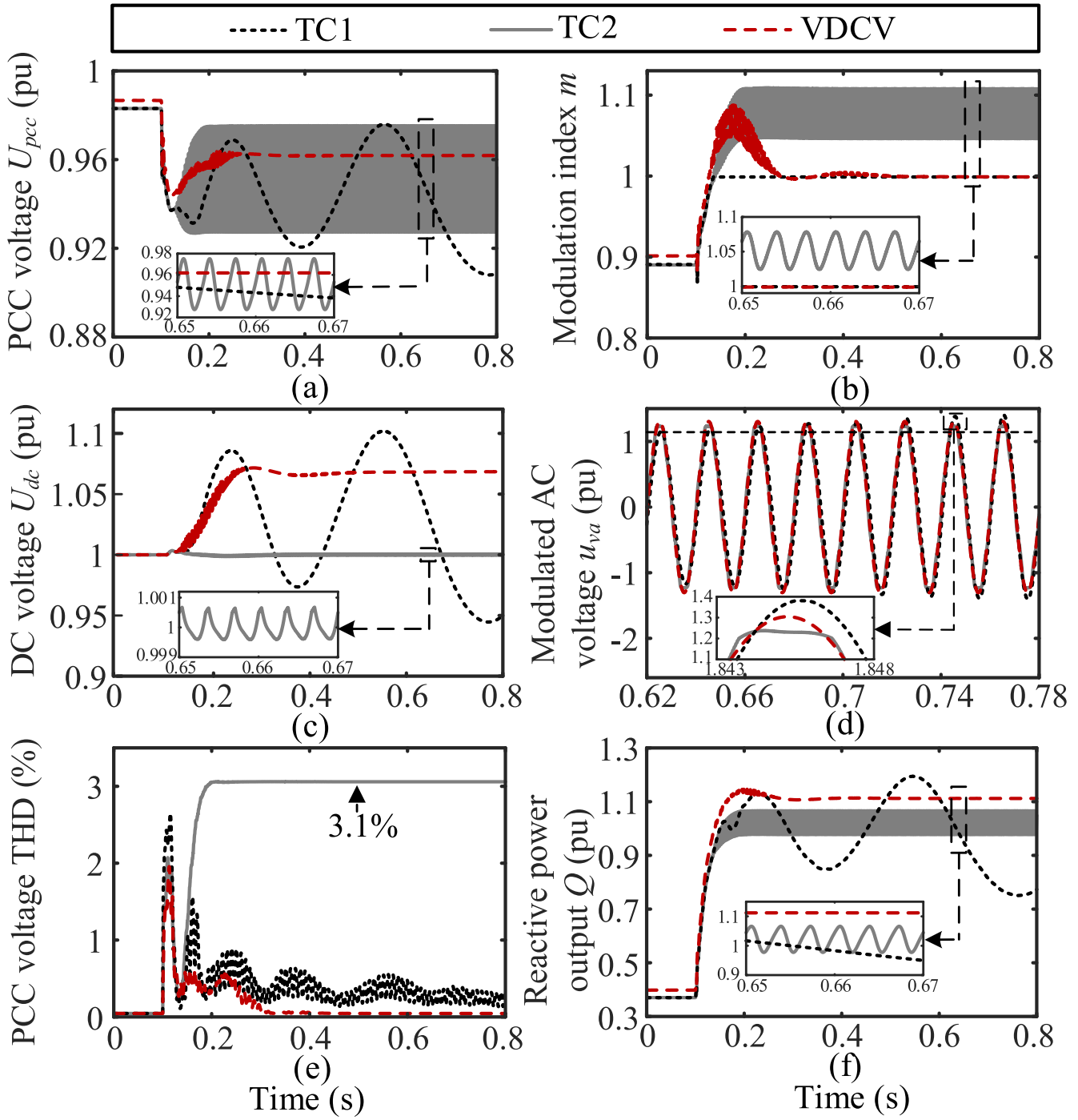

FIGURE 13 Simulation comparison of reactive power load step increase: (a) PCC voltage U_{pcc}, (b) Modulation index m, (c) DC voltage U_{dc}, (d) Modulated AC voltage u_{va}, (e) PCC voltage THD and (f) Reactive power output Q.

STATCOM enters the overmodulation region, as shown in Figure 13b. The overmodulation results in the oscillation of DC voltage and the distortion of the modulated AC voltage, as shown in Figures 13c,d, thus dramatically increasing the THD of the PCC voltage, as shown in Figure 13e. In addition, the overmodulation causes the high-frequency oscillation of the reactive power and the PCC voltage, as shown in Figures 13a,f.

Compared with TC1 and TC2, the VDCV scheme effectively avoids DC voltage oscillation and overmodulation by raising the DC voltage, as shown in Figures 13b,c, thus ensuring the stability of the reactive power and PCC voltage and significantly improving the reactive power output and reducing the PCC voltage drop based on the optimised droop coefficient, as shown in Figures 13a,f.

25152947, 2024, 4, Downloaded from https://ietresearch.onlinelibrary.wiley.com/doi/10.1049/stg2.12147 by NHS Education for Scotland NES, Edinburgh Central Office, Wiley Online Library on [26/08/2024]. See the Terms and Conditions (https://onlinelibrary.wiley.com/terms-and-conditions) on Wiley Online Library for rules of use; OA articles are governed by the applicable Creative Commons License

6.2 | Scenario 2: AC grid three phase ground fault

A temporary 300 ms three-phase fault occurs at the AC grid bus at $t = 0.1$s, which results in a 5% voltage drop of the PCC voltage, as shown in Figure 14a. Compared with TC1 and TC2, VDCV controls the modulation index at its limit by increasing the DC voltage, avoids the overmodulation and the triggering of the modulation index limiter and ensures the stability of the modulation index and DC voltage, as shown in Figures 14b,c. Figures 14d,e show that VDCV expands the adjustable range of the modulated AC voltage, which avoids the distortion of the PCC voltage and reduces its THD to around 0. As seen in Figures 14a,f, VDCV ensures the stability of the reactive power

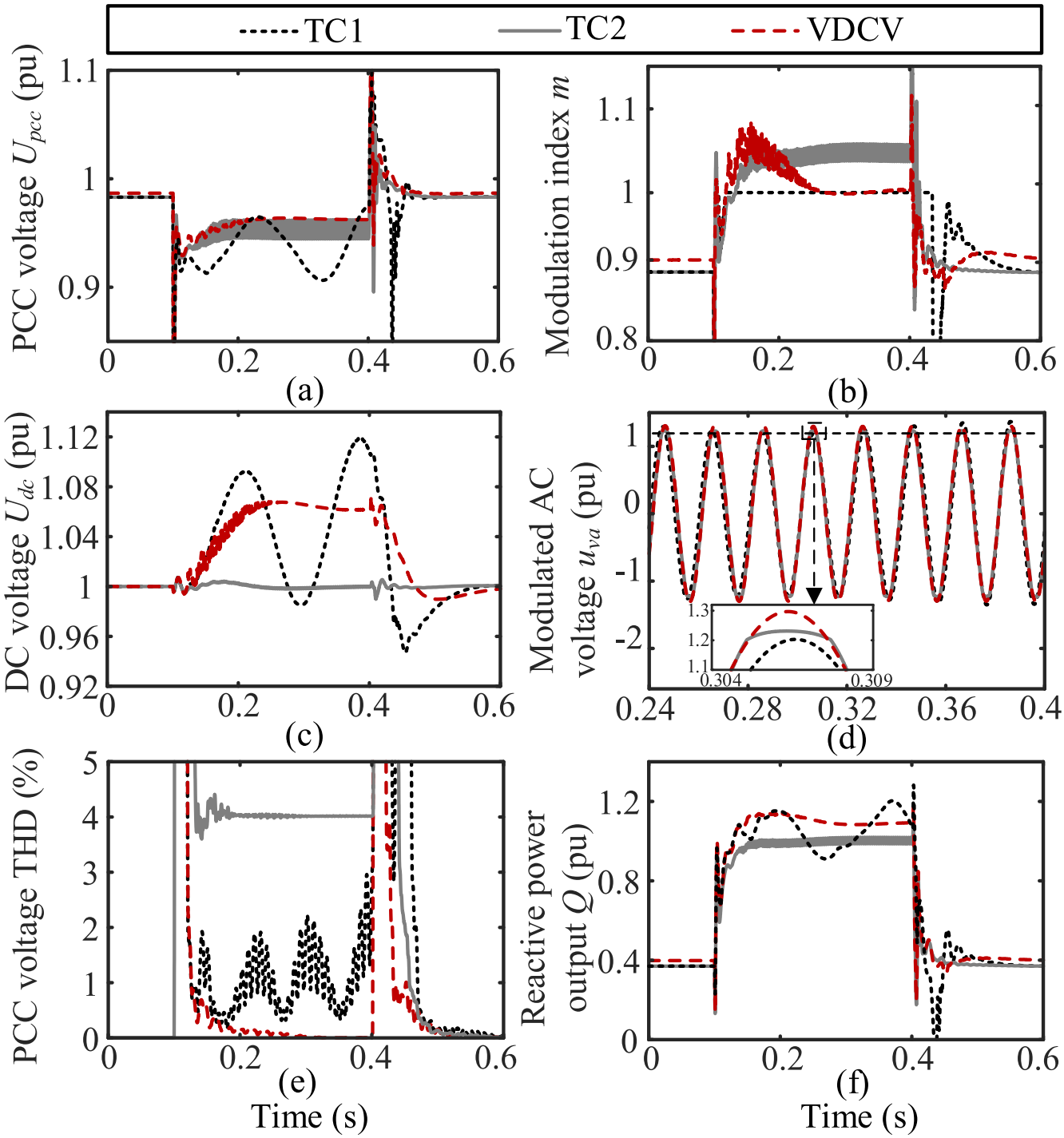

FIGURE 14 Simulation comparison of AC grid three phase transient fault: (a) PCC voltage U_{pcc}, (b) Modulation index m, (c) DC voltage U_{dc}, (d) Modulated AC voltage u_{va}, (e) PCC voltage THD, (f) Reactive power output Q.

25152947, 2024, 4, Downloaded from https://ietresearch.onlinelibrary.wiley.com/doi/10.1049/stg2.12147 by NHS Education for Scotland NES, Edinburgh Central Office, Wiley Online Library on [26/08/2024]. See the Terms and Conditions (https://onlinelibrary.wiley.com/terms-and-conditions) on Wiley Online Library for rules of use; OA articles are governed by the applicable Creative Commons License

output and the PCC voltage, and with the optimised droop coefficient, the reactive power output and the PCC voltage performance are significantly improved.

7 | CONCLUSION

Considering the constraint of the modulated AC voltage, the reactive power output of MMC-STATCOM is potentially unstable under grid contingencies. This paper proposes a variable DC voltage (VDCV)-based reactive power enhancement scheme for MMC-STATCOM. With the designed variable DC voltage control, the DC voltage is effectively increased in a transient state to diminish the constraint of the modulated AC voltage amplitude, providing the advantages of RPC improvement and overmodulation avoidance. The optimisation algorithm adjusts the reactive current-AC voltage droop coefficient, enabling the MMC-STATCOM to make full use of its improved RPC. Small signal analysis conducted obtains the suitable parameters for the proposed VDCV scheme. The theoretical analysis and hardware-in-the-loop results verify the effectiveness of the proposed VDCV scheme in improving the RPC and the voltage support of MMC-STATCOM.

AUTHOR CONTRIBUTIONS

Lujie Yu: Project administration; conceptualisation; writing – review and editing. **Guoyan Wang**: Formal analysis; roles/writing – original draft. **Tong Wu**: Conceptualisation; roles/writing – original draft. **Jiebei Zhu**: Writing–review and editing; supervision. **Campbell D. Booth**: Project administration.

CONFLICT OF INTEREST STATEMENT

The authors declare no conflicts of interest.

DATA AVAILABILITY STATEMENT

The data that support the findings of this study are available from the corresponding author upon reasonable request.

PERMISSION TO REPRODUCE MATERIALS FROM OTHER SOURCES

None.

ORCID

Lujie Yu https://orcid.org/0000-0002-0889-7751
Tong Wu https://orcid.org/0009-0002-3983-3256
Jiebei Zhu https://orcid.org/0000-0002-8591-1123

REFERENCES

1. Aghdam, M.M., Li, L., Zhu, J.: Comprehensive study of finite control set model predictive control algorithms for power converter control in microgrids. IET Smart Grid 3(1), 1–10 (2020). https://doi.org/10.1049/iet-stg.2018.0237
2. Cupertino, A.F., et al.: High performance simulation models for ES-STATCOM based on modular multilevel converters. IEEE Trans. Energy Convers. 35(1), 474–483 (2020). https://doi.org/10.1109/tec.2020.2967314
3. do Carmo Mendonça, D., et al.: Minimum cell operation control for power loss reduction in MMC-based STATCOM. IEEE Trans. Emerg Convers. 9(2), 1938–1950 (2020). https://doi.org/10.1109/jestpe.2020.2979123
4. Chivukula, A.B., Maiti, S.: Analysis and control of modular multilevel converter-based E-STATCOM to integrate large wind farms with the grid. IET Gener. Transm. Distrib. 13(20), 4604–4616 (2019). https://doi.org/10.1049/iet-gtd.2018.5928
5. Das, J.C.: Application of STATCOM to an industrial distribution system connected to a weak utility system. IEEE Trans. Ind. Appl. 52(6), 5345–5354 (2016). https://doi.org/10.1109/tia.2016.2600657
6. Shobana, S., Tamil Selvi, K., Abirami, P.: Implementation of voltage stability system in distribution network by using D-STATCOM. Int. J. Recent Technol. Eng., 2277–3878 (2019)
7. China Electric Power Press, DL/T 1215.1-2013: Chain Static Synchronous Compensator Part 1: Guide for the Functional Specification, 2011
8. Song, Y.H., Johns, A.T.: Flexible Ac Transmission Systems (FACTS): Application Examples of STATCOM. CIGRE Green Books, Switzerland (2020). ISBN: 978-3-030-35386-5
9. Rodriguez-Bernuz, J.M., Junyent-Ferré, A.: Operating region extension of a modular multilevel converter using model predictive control: a single phase analysis. IEEE Trans. Power Delivery 35(1), 171–182 (2019). https://doi.org/10.1109/tpwrd.2019.2908695
10. Kim, H., et al.: Operating region of modular multilevel converter for HVDC with controlled second-order harmonic circulating current: Elaborating PQ capability. IEEE Trans. Power Delivery 31(2), 493–502 (2015). https://doi.org/10.1109/tpwrd.2015.2458038
11. Zhang, Z., et al.: Operating area for modular multilevel converter based high-voltage direct current systems. IET Renewable Power Gener. 10(6), 776–787 (2016). https://doi.org/10.1049/iet-rpg.2015.0342
12. Hao, Q., et al.: Operation and control of MMC station with constraints of internal variables under unbalanced grid conditions. IET Gener. Transm. Distrib. 14(10), 1829–1841 (2020). https://doi.org/10.1049/iet-gtd.2019.1450
13. Wang, J., et al.: Steady-state power operation region of a modular multilevel converter connecting to an AC grid. High Volt. 6(6), 1009–1023 (2021). https://doi.org/10.1049/hve2.12100
14. Li, B., et al.: Research on the power distribution region and multiple constraint matching of modular multilevel converter. Int. Trans. Electr. Energy Syst. 31(8), e12960 (2021). https://doi.org/10.1002/2050-7038.12960
15. IEEE recommended practices and requirements for harmonic control in electrical power systems. IEEE Std 519-1992, 5–10 (1993)
16. Planning levels for harmonic voltage distortion and the connection of non-linear equipment to transmission systems and distribution networks in the United Kingdom. Eng. Recommendation G5/4 (2001)
17. State Bureau of Quality and Technical Supervision, GB/T 14549–1993: Quality of Electric Energy Harmonics in Public Grid (1993)
18. Shi, X., et al.: Capacitor-voltage regulation and linear-range extension of a hybrid cascaded modular multilevel converter. IET Gener. Transm. Distrib. 11(18), 4588–4598 (2017). https://doi.org/10.1049/iet-gtd.2017.0419
19. Huang, M., et al.: Modified modular multilevel converter with third-order harmonic voltage injection to reduce submodule capacitor voltage ripples. IEEE Trans. Power Electron. 36(6), 7074–7086 (2020). https://doi.org/10.1109/tpel.2020.3035286
20. Oghorada, O.J., Zhang, L.: Unbalanced and reactive load compensation using MMCC-based SATCOMs with third-harmonic injection. IEEE Trans. Ind. Electron. 66(4), 2891–2902 (2018). https://doi.org/10.1109/tie.2018.2849962
21. Bin, Y., et al.: Influences of third harmonic injection on the operation characteristics of MMC system. High Volt. Eng. 46(03), 1060–1068 (2020)
22. Guo, G., et al.: Application of third-order harmonic voltage injection in a modular multilevel converter. IEEE Trans. Ind. Electron. 65(7), 5260–5271 (2017). https://doi.org/10.1109/tie.2017.2777413
23. Xu, Y., Li, F.: Adaptive PI control of STATCOM for voltage regulation. IEEE Trans. Power Delivery 29(3), 1002–1011 (2014). https://doi.org/10.1109/tpwrd.2013.2291576
24. Xu, C., et al.: Research on PCC voltage droop control of STATCOM based on modular multilevel converters. Proc. CSEE 35(S1), 205–212 (2015)

25152947, 2024, 4, Downloaded from https://ietresearch.onlinelibrary.wiley.com/doi/10.1049/stg2.12147 by NHS Education for Scotland NES, Edinburgh Central Office, Wiley Online Library on [26/08/2024]. See the Terms and Conditions (https://onlinelibrary.wiley.com/terms-and-conditions) on Wiley Online Library for rules of use; OA articles are governed by the applicable Creative Commons License

25. Li, X., et al.: Performance analysis and optimization of circulating current control for modular multilevel converter. IEEE Trans. Ind. Electron. 63(2), 716–727 (2015). https://doi.org/10.1109/tie.2015.2480748
26. Chen, Y., et al.: Accurate and general small-signal impedance model of LCC-HVDC in sequence frame. IEEE Trans. Power Deliv. 38(6), 4226–4241 (2023). https://doi.org/10.1109/tpwrd.2023.3307552

How to cite this article: Yu, L., et al.: Variable DC voltage based reactive power enhancement scheme for MMC-STATCOM. IET Smart Grid. 7(4), 427–441 (2024). https://doi.org/10.1049/stg2.12147

APPENDIX A

SIMULATION AND CONTROL SYSTEM PARAMETERS

See Tables A1 and A2.

TABLE A1 Simulation system parameters.

Module	Item	Value
MMC-STATCOM	SM number per arm N	32
	SM capacitance C	4.95 mF
	Arm inductance L_0	20 mH
	Carrier frequency f_c	1.05 kHz
	Rated dc voltage U_{dc0}	64 kV
	Rated output ac voltage U_{v0}	32 kV
	Rated PCC voltage U_{pcc0}	230 kV
	Transformer ratio	32/230 kV
	Transformer inductance L_t	10 mH
	Rated Apparent power S	47.5 MVar
	Maximum ac current $I_{\max}$	1286 A
	Droop coefficient k_d	0.045
AC grid system	AC grid voltage	230 kV
	AC equivalent inductance L_s	250 mH
	SCR	4

TABLE A2 Control system parameters.

Parameter	Value
DC voltage outer controller loop (k_{p1}, k_{i1})	(8, 400)
Droop controller loop (k_{p2}, k_{i2})	(1, 100)
Inner current controller loop (k_{p3}, k_{i3})	(0.5, 50)
Circulating current suppression controller loop (k_{p4}, k_{i4})	(0.5, 50)
PLL (k_{p5}, k_{i5})	(60, 1400)
Modulation index controller loop (k_p, k_i)	(0.5, 40)

APPENDIX B

MMC-STATCOM STATE SPACE EQUATIONS

The small signal modelling of MMC-STATCOM mainly includes four parts: MMC main circuit, MMC control system, transformer and coordinate transformation. The state-space equations of each part is as follows:

1) State space equations of MMC main circuit:

① Sub-module capacitor voltage fluctuation dynamic DC component:

$$\frac{d\overline{u_c}}{dt}=\frac{u_{vq}i_q}{4CU_{dc}}+\frac{u_{vd}i_d}{4CU_{dc}}+\frac{u_{cirq}i_{cirq}}{2CU_{dc}}+\frac{u_{cird}i_{cird}}{2CU_{dc}} \tag{B1}$$

where $\overline{u_c}$ is the DC component of capacitor voltage; u_{vdq} is the modulated AC voltage in dq-axis; i_{dq} is the PCC current in dq-axis; u_{cirdq} is the output voltage of the circulating current suppression controller in dq-axis; i_{cirdq} is the circulating current in dq-axis.
Fundamental component:

$$\begin{cases}\dfrac{du_{c\_1d}}{dt}=-\omega u_{c\_1q}-\dfrac{i_d}{4C}-\dfrac{u_{vq}i_{cirq}}{2CU_{dc}}-\dfrac{u_{vd}i_{cird}}{2CU_{dc}}-\\ \qquad\dfrac{u_{cirq}i_q}{4CU_{dc}}-\dfrac{u_{cird}i_d}{4CU_{dc}}\\ \dfrac{du_{c\_1q}}{dt}=-\omega u_{c\_1d}-\dfrac{i_q}{4C}-\dfrac{u_{vd}i_{cirq}}{2CU_{dc}}+\dfrac{u_{vq}i_{cird}}{2CU_{dc}}-\\ \qquad\dfrac{u_{cirq}i_d}{4CU_{dc}}+\dfrac{u_{cird}i_q}{4CU_{dc}}\end{cases} \tag{B2}$$

where u_{c_1dq} is the fundamental frequency component of capacitor voltage in dq-axis.
Second harmonic component:

$$\begin{cases}\dfrac{du_{c\_2d}}{dt}=-2\omega u_{c\_2q}+\dfrac{i_{cird}}{2C}-\dfrac{u_{vq}i_q}{4CU_{dc}}+\dfrac{u_{vd}i_d}{4CU_{dc}}\\ \dfrac{du_{c\_2q}}{dt}=2\omega u_{c\_2d}+\dfrac{i_{cirq}}{2C}+\dfrac{u_{vd}i_d}{4CU_{dc}}+\dfrac{u_{vq}i_q}{4CU_{dc}}\end{cases} \tag{B3}$$

where u_{c_2dq} is the second harmonic component of capacitor voltage in dq-axis.
Third harmonic component:

25152947, 2024, 4, Downloaded from https://ietresearch.onlinelibrary.wiley.com/doi/10.1049/stg2.12147 by NHS Education for Scotland NES, Edinburgh Central Office, Wiley Online Library on [26/08/2024]. See the Terms and Conditions (https://onlinelibrary.wiley.com/terms-and-conditions) on Wiley Online Library for rules of use; OA articles are governed by the applicable Creative Commons License

$$\begin{cases} \dfrac{du_{c\_3x}}{dt} = 3\omega u_{c\_3y} - \dfrac{i_{cirq}u_{vd}}{2CU_{dc}} - \dfrac{i_{cird}u_{vq}}{2CU_{dc}} - \\ \qquad \dfrac{u_{cird}i_q}{4CU_{dc}} - \dfrac{u_{cirq}i_d}{4CU_{dc}} \\ \dfrac{du_{c\_3y}}{dt} = -3\omega u_{c\_3x} + \dfrac{i_{cirq}u_{vq}}{2CU_{dc}} - \dfrac{i_{cird}u_{vd}}{2CU_{dc}} + \\ \qquad \dfrac{u_{cirq}i_q}{4CU_{dc}} - \dfrac{u_{cird}i_d}{4CU_{dc}} \end{cases} \tag{B4}$$

where u_{c_3xy} is the third harmonic component of capacitor voltage in dq-axis.

② DC voltage dynamic:

$$U_{dc} = N\overline{u_c} - \frac{Nu_{cq}u_{c\_1q}}{U_{dc}} - \frac{Nu_{cd}u_{c\_1d}}{U_{dc}} + \frac{Nu_{cirq}u_{c\_2q}}{U_{dc}} + \frac{Nu_{cird}u_{c\_2d}}{U_{dc}} \tag{B5}$$

③ AC current dynamic:

$$\begin{cases} \dfrac{di_d}{dt} = \dfrac{u_{sd}}{L_{eq}} + \dfrac{Nu_{c\_1d}}{2L_{eq}} - N\dfrac{2\overline{u_c}u_{vd} + u_{vq}u_{c\_2q} + u_{vd}u_{c\_2q}}{2L_{eq}U_{dc}} + \\ \qquad N\dfrac{u_{cirq}u_{c\_1q} + u_{cird}u_{c\_1d} + u_{c\_3x}u_{cirq} + u_{c\_3y}u_{cird}}{2L_{eq}U_{dc}} - \omega i_q \\ \dfrac{di_q}{dt} = \dfrac{u_{sq}}{L_{eq}} + \dfrac{Nu_{c\_1q}}{2L_{eq}} - N\dfrac{2\overline{u_c}u_{vq} + u_{vd}u_{c\_2q} - u_{vq}u_{c\_2d}}{2L_{eq}U_{dc}} + \\ \qquad N\dfrac{u_{cirq}u_{c\_1d} - u_{cird}u_{c\_1q} + u_{c\_3x}u_{cird} - u_{c\_3y}u_{cirq}}{2L_{eq}U_{dc}} + \omega i_d \end{cases} \tag{B6}$$

④ Circulating current dynamic:

$$\begin{cases} \dfrac{di_{cird}}{dt} = -2\omega i_{cirq} - \dfrac{Nu_{c\_2d}}{2L_{arm}} - \dfrac{N\overline{u_c}u_{cird}}{L_{arm}U_{dc}} + \\ \qquad \dfrac{Nu_{vd}u_{c\_1d} - Nu_{vq}u_{c\_1q} + Nu_{c\_3x}u_{vq} + Nu_{c\_3y}u_{vd}}{2L_{arm}U_{dc}} \\ \dfrac{di_{cirq}}{dt} = -2\omega i_{cird} - \dfrac{Nu_{c\_2q}}{2L_{arm}} - \dfrac{N\overline{u_c}u_{cirq}}{L_{arm}U_{dc}} + \\ \qquad \dfrac{Nu_{vd}u_{c\_1q} + Nu_{vq}u_{c\_1d} + Nu_{c\_3x}u_{vd} + Nu_{c\_3y}u_{vq}}{2L_{arm}U_{dc}} \end{cases} \tag{B7}$$

The small signal model of MMC uses u_{vdq}, ω, u_{cirdq} as its input variables, which provides interface for inner current controller loop, PLL controller and circulating current suppression controller loop respectively; u_{sdq} provides the interface with AC system; U_{dc} provides the interface with DC system.

2) State space equations of MMC control system:

① Outer controller loop

$$\begin{cases} i_d^* = \left(k_{p1} + \dfrac{k_{i1}}{s}\right)\left(U_{dc} - U_{dc}^*\right) \\ i_q^* = \left(k_{p2} + \dfrac{k_{i2}}{s}\right)\left(U_{pcc} - U_{pcc}{}^*\right) \\ U_{pcc}{}^* = 1 + k_d i_q^* \end{cases} \tag{B8}$$

where $i_{dq}{}^*$ is the PCC current reference in dq-axis.

② Inner current controller loop

25152947, 2024, 4, Downloaded from https://ietresearch.onlinelibrary.wiley.com/doi/10.1049/stg2.12147 by NHS Education for Scotland NES, Edinburgh Central Office, Wiley Online Library on [26/08/2024]. See the Terms and Conditions (https://onlinelibrary.wiley.com/terms-and-conditions) on Wiley Online Library for rules of use; OA articles are governed by the applicable Creative Commons License

$$\begin{cases} u_{vd} = \left(k_{p3} + \dfrac{k_{i3}}{s}\right)\left(i_d^* - i_d\right) - \omega L_{eq} i_q + u_{pccd} \\ u_{vq} = \left(k_{p3} + \dfrac{k_{i3}}{s}\right)\left(i_q^* - i_q\right) + \omega L_{eq} i_d + u_{pccq} \end{cases} \tag{B9}$$

where u_{vdq}* is the modulated AC voltage reference in dq-axis. u_{pccdq}* is the PCC voltage reference in dq-axis.

③ Circulating current suppression controller loop

$$\begin{cases} {i_{cird}}^* = 0, {i_{cirq}}^* = 0 \\ u_{cird} = -\left(k_{p4} + k_{i4}/s\right)\left({i_{cird}}^* - i_{cird}\right) - 2\omega L_0 i_{cirq} \\ u_{cirq} = \left(k_{p4} + k_{i4}/s\right)\left({i_{cirq}}^* - i_{cirq}\right) + 2\omega L_0 i_{cird} \end{cases} \tag{B10}$$

where i_{cirdq}* is the circulating current reference in dq-axis; u_{cirdq}* is the output voltage reference of the circulating current suppression controller in dq-axis.

④ PLL controller

$$\begin{cases} \theta = \dfrac{\omega}{s} \\ \omega = \left(k_{p5} + \dfrac{k_{i5}}{s}\right) u_{pccq} \end{cases} \tag{B11}$$

3) State space equations of the transformer:

$$\begin{cases} \dfrac{di_d}{dt} = \omega i_q - \dfrac{R_t}{L_t} i_d + \dfrac{u_{td} - u_{t1d}}{L_t} \\ \dfrac{di_q}{dt} = -\omega i_d - \dfrac{R_t}{L_t} i_q + \dfrac{u_{tq} - u_{t1q}}{L_t} \end{cases} \tag{B12}$$

where L_t and R_t are the equivalent inductance and resistance of the transformer, respectively; u_{tdq} and u_{t1dq} are the voltage on both sides of the transformer in dq-axis.

APPENDIX C

MAIN EIGENVALUES OF MMC-STATCOM CONNECTED SYSTEM

See Table C1.

TABLE C1 Main eigenvalues of the MMC-STATCOM connected system.

λ	Eigenvalue	Damping ratio	Frequency (Hz)
λ_1	−185,840	1	0
λ_2	−17,670	1	0
$\lambda_{3,4}$	−15620±j632.89	0.9992	100.7280
$\lambda_{5,6}$	−875.02±j2341.8	0.35	372.7135
$\lambda_{7,8}$	−209.78±j1919.3	0.1087	305.4703
$\lambda_{9,10}$	−275.46±j122.03	0.9143	19.421
$\lambda_{11,12}$	−31.740±j115.58	0.2648	18.3950
$\lambda_{13,14}$	−26.62±j20.83	0.7877	3.3146
$\lambda_{15,16}$	−35.95±j6.9	0.9821	1.0988
λ_{17}	−64.05	1	0
$\lambda_{18,19}$	−119.19±j24.4	0.9797	3.8841
λ_{20}	−127.21	1	0
λ_{21}	−96.7	1	0
λ_{22}	−103.24	1	0

25152947, 2024, 4, Downloaded from https://ietresearch.onlinelibrary.wiley.com/doi/10.1049/stg2.12147 by NHS Education for Scotland NES, Edinburgh Central Office, Wiley Online Library on [26/08/2024]. See the Terms and Conditions (https://onlinelibrary.wiley.com/terms-and-conditions) on Wiley Online Library for rules of use; OA articles are governed by the applicable Creative Commons License